Scour patterns around isolated vegetation elements

Oral Yagci[a], Mehmet Furkan Celik[b], Vasileios Kitsikoudis[a], V.S. Ozgur Kirca[a], Can Hodoglu[a], Manousos Valyrakis[c], Zaide Duran[b], Sinasi Kaya[b]

[a]*Division of Hydraulics, Civil Engineering Department, Civil Engineering Faculty, Istanbul Technical University, Maslak 34469, Istanbul, Turkey*
[b]*Geomatics Engineering Department, Civil Engineering Faculty, Istanbul Technical University, Maslak 34469, Istanbul, Turkey*
[c]*Infrastructure and Environment Research Division, School of Engineering, University of Glasgow, Glasgow G12 8LT, UK*

Abstract

The complex multi-directional interactions between hydrological, biological and fluvial processes govern the formation and evolution of river landscapes. In this context, as key geomorphological agents, riparian trees are particularly important in trapping sediment and constructing distinct landforms, which subsequently evolve to larger ones. The primary objective of this paper is to experimentally investigate the scour/deposition patterns around different forms of individual vegetation elements. Flume experiments were conducted in which the scour patterns around different representative forms of individual in-stream obstructions (solid cylinder, hexagonal array of circular cylinders, several forms of emergent and submerged vegetation) were monitored by means of a high-resolution laser scanner. The three dimensional scour geometry around the simulated vegetation elements was quantified and discussed based on the introduced dimensionless morphometric characteristics. The findings reveal that the intact vegetation forms generated two elongated scour holes at the downstream with a pronounced ridge. For the impermeable form of the plant, the scour got localized, more deposition was detected within the monitoring zone, and the distance between the obstruction and deposition zone became shorter. It is also shown that with the effect of bending and the subsequent decrease of the projected area of the plant and the increase of bulk volume, the characteristic scour values decrease compared to the intact version, and the scour zone obtains a more elongated form and expands in the downstream direction.

Keywords:

Flow-vegetation interaction, individual vegetation elements, local scour, pioneer islands,

riparian trees, scour geometry

1. Introduction

Knowledge about the intertwined interactions among water-biota-sediment in natural rivers is one of the central issues in todays sustainable river management. The problem framework has been classified at different scales, namely the planform, reach and individual scale [1–3].

At planform scale, the multi-directional relations among hydrological, biological and fluvial processes in natural waterways dictate the formation and evolution of river landscapes [4–7]. Riparian plants are key geomorphological agents, ubiquitous at the interface between terrestrial and aquatic zone, and regulate the fluxes of water, nutrient, sediment and organic matter along river corridors [8–14]. Moreover, it is a well-documented fact that riparian vegetation is capable of accelerating the recovery of poorly managed river channels [15–17]. The experimental study by Tal and Paola [18] clearly demonstrated how the pattern of a river system evolves from braided to single thread under the impact of a repeated cycle of discharge fluctuations and its influence on vegetation. Once the individual/patch of vegetation gets established, it triggers the initiation of morphological changes through the development of pioneer landforms. According to Gurnell et al. [19], riparian vegetation is particularly effective in trapping transported sediment, which could lead to the development of vegetated islands, and/or the expansion of river banks and floodplains. Riparian vegetation has also considerable influence on the hydraulic geometry of natural rivers [20, 21]. With all the other factors being equal, rivers with dense vegetation communities tend to generate deeper and narrower (according to Ikeda and Izumi [22], 30% narrower) channel geometries compared to their sparsely vegetated counterparts [23, 24]. Tsujimoto [25] suggested a rotational degradation concept, which denotes a stress and velocity reduction around the vegetation strip, encouraging vegetation to spread through lateral expansion. This brings about increase in velocities and shear stresses in the main channel and consequently narrowing of the channel width.

A significant emphasis is given to the problem also at the reach scale. In the past, hydraulic engineers traditionally regarded the riparian and aquatic vegetation as a source of additional resistance to flow and tended to remove them from the waterways. However, since the beneficial impact of vegetation on the riverine ecosystem is now widely acknowledged, there is an apparent need to properly estimate the consequent flow alteration. Especially for the flood mapping studies, it is required to estimate vegetation induced resistance with an acceptable accuracy for high-intensity-low-frequency floods. Brierly and Fryirs [26] argued that the proportion of vegetation occupying a channel cross-section decreases downstream as the channel becomes wider. Also its existence alters not only the hydraulic resistance but also the velocity distribution [27–31], turbulence patterns [32, 33], momentum exchange between the main channel and the floodplain [34–38], sediment yield [39–41], and concentration time and groundwater recharge in the basin [42].

At the finer scale (i.e. individual scale) the attention is focused on the flow around/through an individual plant or a patch of vegetation [6, 43–45]. Contrary to the aforementioned reach scale, the flow around an individual plant or a short patch of vegetation is not fully developed. Instead, flow through an individual plant exhibits similarities to the typical flow-body interaction problem, where secondary flow along with some coherent structures are generated in the vicinity of the obstacle. The increase in local shear stress around the vegetation element triggers the formation of the scour/deposition zones around the plant. These individual or patch elements usually expand in the downstream direction. This fact suggests that the generated flow pattern in the vicinity of the vegetation element creates appropriate conditions for deposition behind the vegetation element, which aids patch expansion [46] and consequently plays a role in the generation of streamlined vegetated mid-channel islands. According to Schnauder and Moggridge [47] the intertwined interaction between the deposition, the establishment of plant propagules and the hydraulic characteristics plays a crucial role in initial vegetation establishment. This local fine-scale complex process may lead to the formation of large-scale river planforms in long time scales [48]. Hence, delineation of the interaction between individual plants and the scour/deposition characteristics provides the foundation for the development of successful river rehabilitation strategies. Within the frame of this perspective, the primary objective of this study is to better understand the scour patterns around different forms of vegetal elements and to quantify their morphometric characteristics. As a secondary objective, it is also aimed to provide an interpretation of the coherent flow structures, which are generated around each obstacle, by establishing links between the observed scour patterns and the existing knowledge in the pertinent literature.

Scour and plant characteristics were quantified by means of laser scanner and their interrelation was interpreted. It should be noted that in nature, each vegetation species is unique in terms of their morphometric [49, 50], biomechanical [51] and even seasonal [52] properties. Hence, even the same plant species, when they are exposed to flow, may cause different distinctive coherent structures in their vicinity, depending on age and season, and consequently scour patterns. In the past, a vast amount of research has been conducted to understand the problem of flow-cylindrical structure interaction ranging from the single circular cylinder (which has a relatively well-defined and simple geometry compared to natural vegetation) to more complicated forms of obstacles. Herein, each examined obstacle generates a unique flow pattern around itself. Since it is not practically possible to tackle all the generated flow patterns around each obstacle by flow measurements within a single study, it was aimed to understand/interpret these patterns based on commonly adopted findings in the pertinent literature. Hence, resolving the flow structure around the tested vegetal elements is kept beyond the aim of the present paper.

2. Scope of the study

In a series of 14 experiments conducted within the scope of this study, the scour patterns around different forms of three major types of obstacles were examined: (1) A solid emergent cylinder, (2) a hexagonal array of circular cylinders with an overall diameter equivalent to that of solid cylinder, and (3) different forms of individual natural vegetation elements. Only vegetation with distinct trunks were examined and for the sake of simplicity, hereafter the term ”vegetation” denotes the plant with distinct trunk unless otherwise stated. The geometrical properties of the obstacles and hydraulic conditions of the 14 conducted experiments are summarized in Table 1.

Table 1: Experiment details

Exp. No.	q (l/s/m)*	Obstacle	U_0 (cm/s)	d_{verc} (cm)	Re	Fr	U_f (m/s)	θ	θ/θ_{cr}
1	47	Solid Cylinder	22	16.3	35200	0.10	0.012	0.015	0.38
2	59	Solid Cylinder	25	16.3	40750	0.11	0.014	0.017	0.43
3	85	Solid Cylinder	37	16.3	60310	0.16	0.021	0.037	0.93
4	59	Hexagonal Cylinder	25	9.4	23500	0.11	0.014	0.017	0.43
5	85	Hexagonal Cylinder	37	9.4	34780	0.16	0.021	0.037	0.93
6	59	Emergent Vegetation	25	3.1	7750	0.11	0.014	0.017	0.43
7	85	Emergent Vegetation	37	3.1	11470	0.16	0.021	0.037	0.93
8	59	Impermeable Emergent Vegetation	25	13.1	32750	0.11	0.013	0.017	0.43
9	59	Bended Emergent Vegetation	25	N/A	N/A	0.11	0.013	0.017	0.43
10	85	Bended Emergent Vegetation	37	N/A	N/A	0.16	0.021	0.037	0.93
11	59	Submerged Vegetation	25	2.34	5850	0.11	0.013	0.017	0.43
12	85	Submerged Vegetation	37	2.34	8658	0.16	0.021	0.037	0.93
13	59	Impermeable Submerged Vegetation	25	12.97	32425	0.11	0.014	0.017	0.43
14	85	Impermeable Submerged Vegetation	37	12.97	47989	0.16	0.021	0.037	0.93

* ±3 l/s/m

First three experiments were conducted for a solid emergent cylinder. The experimental runs with this well-known obstacle serve as benchmark for the other runs that utilize more complicated obstacles, since the scour around an emergent rigid cylinder has been extensively studied so far [53–57], hence considerable knowledge exists in the pertinent literature.

A hexagonal array of circular cylinders (HACC) was utilized to simulate a permeable version of the rigid cylinder as previously done by Valyrakis et al. [58]. This form can be considered as a transition case from rigid emergent cylinder to emergent vegetation, but closer to cylinder due to the absence of subcanopy flow. The employed HACC consisted of seven equally distant identical cylinders located at the corners and the center of a regular hexagon.

Flow energy reaches its maximum level during the passage of formative floods (i.e. discharges with high returning period), which is adequately high to affect the river morphology. The definition of the formative flood changes depending on the flow features observed in a river [21]. While the channel dimensions are heavily dictated by floods where the annual discharge patterns are characterized by sharp flood peaks, in rivers with more regular annual discharge patterns the dimensions of the channel are highly controlled by mean annual flows [59]. However, it is demonstrated that the channel dimensions are dictated not only by the discharge characteristics (by the peak values and the temporal distribution of the discharge) but also the existing vegetation cover and the sediment features [60]. Usually bank/floodplain and mid-channel vegetation with distinct trunk is in emergent form when they are exposed to flow during these formative floods. The scour process around the emergent vegetation has certain indirect effects on biogeomorphology [48], among others as detailed below, and this constituted the main underlying motivation in conducting emergent vegetation experiments in the present campaign (experiment no. 6 and 7 in Table 1).

As firstly pointed out by Schnauder et al. [61], permeability of a plant canopy is one of the most influential features of the plant morphology since it heavily influences the flow field around a single vegetal element (contraction, downflow, bleed-flow, subcanopy flow, horse-shoe vortex, and stem scale lee-wake vortices). Therefore, the role of plant permeability on scour patterns arises as an important question. From this motivation, the scour pattern was investigated for two distinct configurations of the same plant (*Cupressus Macrocarpa*); namely its intact form and with its canopy wrapped with impermeable stretch-film, as firstly done in [61] (experiment no. 8, 13, and 14 in Table 1).

In nature, especially when formative floods take place, water level rises such that the natural plants on distinct pioneer islands and the ones located at the higher elevations of the bank/floodplain are exposed to significant hydrodynamic forcing. As a result of this, they are bended, compressed, and attain a shape that is streamlined with the flow [44, 61–63]. In order to achieve a better understanding of the influence of bending/compressing of vegetation on the scour pattern, the previously tested emergent vegetation was artificially bended by an external force (as conceptually firstly done in [64]) and exposed to similar flow conditions (experiment no. 9 and 10 in Table 1).

The term submerged vegetation is an umbrella term and it denotes a wide range of species. The flow-submerged vegetation interaction at the reach scale (i.e. fully developed flow conditions) has been studied relatively more extensively [27, 31, 62, 65–67] compared to the emergent case. Nevertheless, the knowledge gained regarding the scour around submerged individual tree-like plants with high flexural rigidity is inadequate. In the light of this argument, the submerged vegetation case was included into the scope of the present experimental program (experiment no. 11 and 12 in Table 1). In addition to the intact submerged form, due to the points noted in the preceding paragraph, the impermeable version of the submerged plant was also studied experimentally (i.e. by wrapping it by stretch-film, experiment no. 13 and 14 in Table 1).

3. Experimental setup and procedure

3.1. Flume

All the experiments were conducted in the flow flume located in the Hydraulics Laboratory of Istanbul Technical University, which is 26 m long, 0.98 m wide, and 0.85 m deep. The sidewalls of the flume are made of Plexiglas and the bed is smooth concrete. A 12.2 m long false bottom was constructed along the flume that contained a sediment pit, which had a depth of 0.26 m and length of 2.2 m, as shown in Fig. 1. So as to maintain smooth inlet conditions and

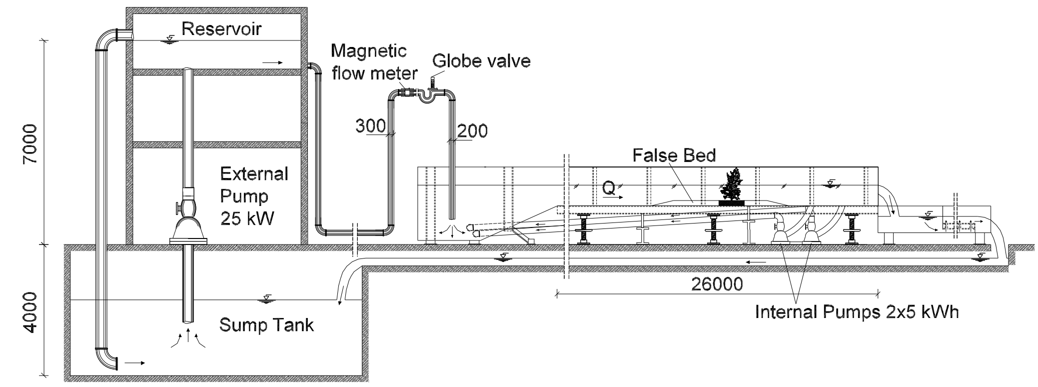

(a)

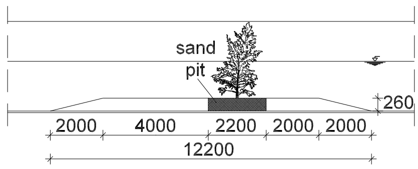

(b)

Figure 1: (a) The utilized flume and (b) the installed false bed with the sand pit. All dimensions are in mm and not to scale.

to prevent unevenness of the water surface elevation across the width, a honeycomb type of flow straightener was placed over the entire width and depth of the flume at its entrance.

The flume is able to provide internal as well as external flow circulation, as can be seen from Fig. 1. Both external and internal circulation systems were utilized simultaneously throughout the experiments to achieve the required flow velocity. At the end of the flume, a tailgate weir controlled the flow depth. The external circulation provided flow such that the flow passing over the tailgate weir was discharged into a steel stilling basin. The water from the stilling basin was discharged into an internal canal system of the hydraulics laboratory. The canal system transmitted the water into a large sump tank. With the utilization of a pump, which has power of 25 kW, the water in the sump tank was elevated to a tower reservoir located 7 m above the flume level. Subsequently, the water that was released from the tower reservoir was routed via gravity to the flume through a pipe. For the internal circulation system, a pump with 5 kW power located at the downstream end of the flume was operated.

3.2. Instrumentation

Throughout the undisturbed velocity measurements a Nortek acoustic Doppler velocimeter (ADV) was employed, namely a Vectrino+ that allows 3D data collection at a single point with sampling frequency up to 200 Hz. Vectrino's frequency was set to 50 Hz considering the criterion proposed in [68]. Based on earlier velocity measurement experiences in the same flume [43, 44] a particle rich water environment was provided to obtain better signal-to-noise ratio (SNR) and correlation values. The measured velocity records were post-processed by the despiking methodology suggested in [69] and later on modified in [70].

The utilized laser scanner used in the present study, Leica ScanStation C10, is a motorized total station with a pulse based laser, which measures automatically all the points in the horizontal and vertical field. It is capable of scanning in 360 degrees in horizontal and 270 degrees in vertical. Medium resolution was applied in the present study, which means that the instrument scans the surface with 1 mm grid from 1 m distance.

3.3. Hydraulic conditions

The hydraulic conditions and the obstacle characteristics are summarized in Table 1. All the experiments were conducted for clear water flow conditions (i.e. the bed material was not in motion by the undisturbed flow). Medium sand with median diameter of $d_{50} = 0.7$ mm and standard geometric deviation of $\sigma_g = \sqrt{d_{84}/d_{16}} = 2$ was used in the experiments. In Table 1, in order to make the obstacles comparable with each other in terms of their volume, the submerged volumes of the different obstacles are expressed in terms of the diameter of a volumetrically equivalent rigid cylinder d_{VERC}. In this study, the Reynolds number is described based on the characteristic value of d_{VERC} in order to make the values of Reynolds number for different obstacles comparable. U_0 is the depth averaged velocity where the flow is undisturbed. Throughout the experiments the water depth was set to 23 ± 0.7 cm. The shear velocity, U_f, was calculated using the Colebrook-White equation. The values of Shields parameter, which were calculated according to Eq. (1), are also presented in Table 1.

$$\theta = \frac{\rho U_f^2}{g\,(\rho_s - \rho)\,d} \tag{1}$$

where θ is the Shields parameter, U_f is the shear velocity, ρ and ρ_s is the water and sediment density, respectively, g is the gravitational acceleration, and d is a characteristic grain diameter (median diameter d_{50} was used).

In the solid cylinder experiments, the diameter of the cylinder was 16 cm. The solid cylinder was exposed to different flow discharges resulting in cylinder Reynolds numbers in the range of subcritical regime, $Re = VD/\nu$, where V is the mean flow velocity, D is the cylinder diameter, and ν is the kinematic viscosity. In this regime, for $300 < Re < 3 \times 10^5$, the wake is completely turbulent; however, the cylinder surface boundary layer remains laminar [71].

The primary objective of the study was not to obtain the maximum expected scour depth for equilibrium conditions for the different obstacles. Instead, it was aimed to compare the morphometric properties of the scour patterns that occur under same conditions (i.e. flow strength and test duration) for various obstacles. Thus, the experiments duration was limited to three hours.

3.4. Obstacle characteristics

As stated above, scour around a solid cylinder was studied to provide a reference case for the other examined obstacles. The diameter of the solid emergent cylinder was 16 cm. A hexagonal array of circular cylinders (HACC) was examined as the permeable version of the solid cylinder and was placed in a staggered formation. The overall outer diameter of the cylinder array structure is equal to the solid cylinder, while each of the small cylinders has a 3.4 cm diameter. Fig. 2 shows all the examined obstacles.

Both architectural (i.e. projected area, porosity, submerged volume), and mechanical (i.e. flexural rigidity) characteristics of riparian plants play a significant role on the flow field in the vicinity of the plant. It is important to establish a link between these obstacle characteristics and the flow hydrodynamics. From this motivation, submerged vegetation volume values belonging

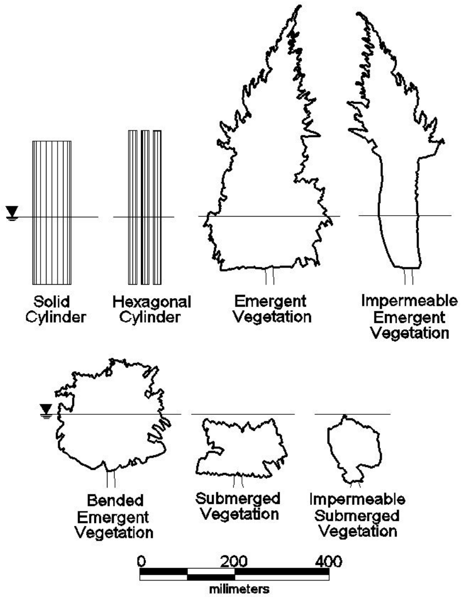

Figure 2: Scaled projection of the obstacles, obtained by laser scanner. Flow is towards the page.

to examined vegetation elements were measured by cutting trees into parts and measuring their volumes by dipping them into a measuring cylinder as firstly done by Schnauder and Moggridge [61]. The variation of cumulative volume of the obstacles with respect to water depth is given in Fig. 3. As can be seen from Fig. 3, differing from the cylinder-like obstacles the variation of the submerged volume with respect to the height for natural vegetation is not linear. There is a change of the slope of the curves both for emergent and submerged vegetation. This can be explained by the fact that the utilized vegetation has two distinct parts, i.e. trunk and canopy.

Bulk (i.e. porosity included) projected area was quantified by means of laser scanner and tabulated in Table 2. In this study, bulk projected area is defined as the area bounded by the outer edge of the vegetation form (identified as point cloud by the laser scanner), which is perpendicular to flow direction (Fig. 2). Moreover, considering its aid in the interpretation of the results, the variation of bulk volume (porosity included) with respect to height was also measured by means of laser scanner. During the calculation of the submerged bulk volume (BV), Eq. 2 was

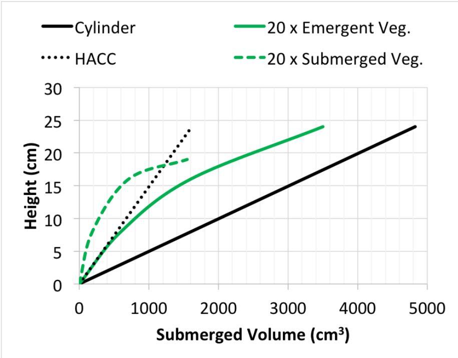

Figure 3: Variation of the cumulative volume of the obstacles with respect to the water depth

employed based on the reference sketch given in Fig. 4(a).

$$\mathrm{BV} = \sum_{i=2}^{n} \frac{a_i + a_{i-1}}{2} \cdot (z_i - z_{i-1}) \tag{2}$$

In Fig. 4(b), the variation of bulk volume of the plants is presented. As can be seen from Fig. 4(b), the bulk volume of the selected emergent vegetation is higher than the submerged one. Also it is obvious that the process of wrapping the plant decreases the bulk volume of both emergent and submerged vegetation. Furthermore, according to Fig. 4(b), when the plant was artificially bended, the bulk volume slightly increases along the depth except in the region closer to the water surface.

The crown ratio (the ratio of tree length supporting live foliage to total tree length [72]) is a useful parameter, which describes the tree-like plant anatomy. The trunk to canopy ratio for the submerged part of the tree is another descriptive parameter, which embodies the plant crown ratio as well as the species age, size, and water level in the open channel. Typical tree-like species in the river active zones are *Salix*, *Populus*, and *Alnus* [73–75], as well as tree vegetation in the rest of the floodplain, e.g., *Ulmus* species [73, 75]. The crown ratio can be over 95% for *Alnus Rubra* [76], *Salix Negra* [77], and several *Populus* [72, 78] species. In this study, the crown ratio value for the submerged portion of the plant was 0.83-0.86 for all the experiments.

The width of the wrapped plant was intentionally reduced, as can be seen from Fig. 2, where

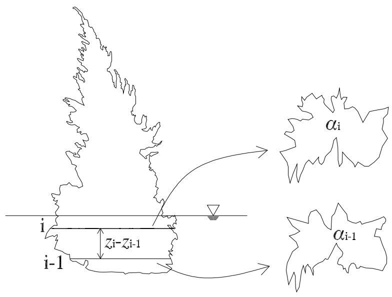

(a)

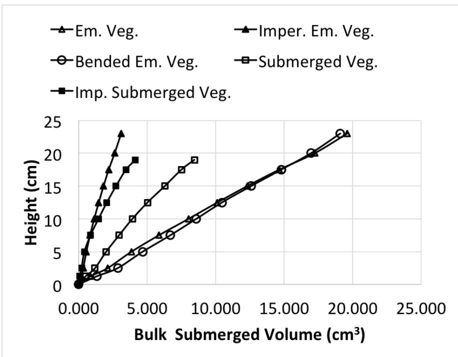

(b)

Figure 4: (a) Definition sketch for the bulk volume calculation and (b) variation of the bulk submerged volume with respect to height. Water surface is at 23±0.7 cm.

the obstacles are given in scaled form. The width of the intact vegetation was significantly larger compared to the other obstacles but due to its high permeability a large portion of the flow was penetrating the plant. If the width of the permeable plant was kept constant during the wrapping process, the sidewall effect would become pronounced, which would prevent the natural development of the scour process. In line with this thought, the width of the plant was intentionally reduced; however, it allowed subcanopy flow to occur, exhibiting a distinguishing feature of tree-like vegetation.

3.5. Procedure

The following experimental procedure was carried out throughout the experimental campaign:

- Mount the vegetative element.
- Level the sediment in the pit to maintain a completely flat bottom.
- Conduct pre-test laser scanning.
- Fill up the flume very slowly (i.e. approximately 3 hours) to prevent initial scouring and maintain full saturation of the sediment.
- Switch on the flow and run the flume for 3 hours.
- Switch off the flow and drain the flume very slowly (i.e. approximately 3 hours) to prevent additional scouring.
- Conduct post-test laser scanning.
- Replace the vegetative element and follow the above steps for the next test.

4. Results and discussion

4.1. Morphometric analysis of the scour/deposition patterns

The contour plots of the scour area for the solid cylinders and the three dimensional scour patterns for the HACC, emergent and submerged vegetative elements are presented in Fig. 5 and

Figs. 6 - 8, respectively. The morphometric quantifications of the scour/deposition patterns were carried out based on the laser scanner measurements and tabulated in Table 2. The examined characteristics observed within the monitoring region are scour depth S_d, scour area in planview S_a, longitudinal scour area along the centerline S_{ac}, longitudinal scour extent at the centerline S_{lc}, scour volume S_v, spanwise width of scour hole S_w, deposition height D_h, deposition area in planview D_a, deposition volume D_v, upstream-slope of scour hole J_{ups}, and side-slope of scour hole J_{side}, which are presented respectively in Table 2. The visual representations of some of the parameters are given on a definition sketch in Fig. 9.

Table 2: Morphometric characteristics of the scour patterns[a]

Exp. No.	Obstacle	$(Vol)_{obs}$ (cm^3)	d_{verc} (cm)	Proj. area (cm^2)	S_d (cm)	S_a (cm^2)	S_{ac} (cm^2)	S_{lc} (cm)	S_v (cm^3)	S_w (cm)	D_h (cm)	D_a (cm^2)	D_v (cm^3)	J_{ups} (%)	J_{side} (%)	P_t (cm)	P_s (-)	P_f (-)	V_R (-)	P_{tc} (cm)
1	Solid Cylinder	4825	16.3	368	6.3	1611	30	18.7	1700	32.3	3.7	1133	800	48.5	55.5	1.1	0.4	0.1	0.5	1.60
2	Solid Cylinder	4825	16.3	368	10.7	5542	301	50.3	12900	53.2	6.9	4288	7111	61.4	55.9	2.3	0.7	0.1	0.6	5.99
3	Solid Cylinder	4825	16.3	368	16.1	7980	538	69.8	26000	62.1	5.1	3242	5976	64.3	57.0	3.3	1.0	0.1	0.2	7.71
4	HACC	1616	9.4	368	8.1	6358	140	34.4	8000	39.8	5.9	3208	4127	52.0	64.7	1.3	0.9	0.1	0.5	4.08
5	HACC	1616	9.4	368	12.4	8712	248	52.3	26800	49.6	3.6	1401	1672	55.3	62.8	3.1	1.3	0.2	0.1	4.74
6	Emergent Vegetation	175	3.1	1100	9.3	6218	103	35.9	12400	42.4	2.3	2679	3833	52.1	50.3	2.0	3.0	0.2	0.3	2.87
7	Emergent Vegetation	175	3.1	1064	12.6	7559	420	69.5	38000	43.1	2.7	183	136	61.8	52.7	5.0	4.1	0.5	0.0	6.04
8	Imper. Emergent Veg.	3100	13.1	345	11	4720	226	49.01	8900	39.3	5.1	1867	3935	64.5	57.7	1.9	0.8	0.1	0.4	4.61
9	Bended Emergent Veg.	N/A	N/A	931	5.4	4321	89	39.5	6500	29.1	2.5	827	914	50.8	49.4	1.5	N/A	0.3	0.1	2.25
10	Bended Emergent Veg.	N/A	N/A	914	10.4	7802	361	71.1	34300	40.3	4.9	523	635	62.2	52.0	4.4	N/A	0.5	0.0	5.08
11	Submerged Vegetation	77	2.34	648	4.2	3850	84	34.5	1800	22.0	1.6	2965	916	41.4	43.2	0.5	1.8	0.2	0.5	2.43
12	Submerged Vegetation	77	2.34	634	8.7	8369	372	80.3	19900	33.5	5.3	1347	1485	43.0	44.1	2.4	3.7	0.5	0.1	4.63
13	Imper. Submerged Veg.	2773	12.97	372	6.9	5721	138	38.5	5100	30.6	5.7	2707	2599	48.8	48.9	0.9	0.5	0.2	0.5	3.58
14	Imper. Submerged Veg.	2773	12.97	387	10.1	9125	313	66.5	18700	44.6	2.3	2071	2857	42.7	43.1	2.0	0.8	0.2	0.2	4.70

[a] $(Vol)_{obs}$ is the submerged volume of the obstacle, d_{verc} is the diameter of volumetrically equivalent rigid cylinder, S_d is the scour depth, S_a is the scour area in planview, S_{ac} is the longitudinal scour area along the centerline, S_{lc} is the longitudinal scour extent at the centerline, S_v is the scour volume, S_w is the scour hole width, D_h is the deposition height, D_a is the deposition area in planview, D_v is the deposition volume, J_{ups} is the upstream slope of the scour hole, J_{side} is the side-slope of the scour hole.

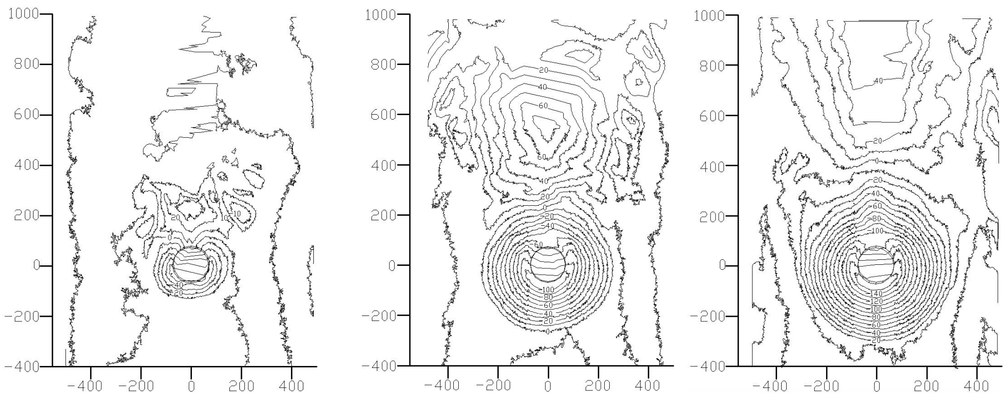

(a) (b) (c)

Figure 5: Contour plots of the scour pattern for flow over solid cylinder for the three discharges shown in Table 1 (a) 47 l/s/m, (b) 59 l/s/m, and (c) 85 l/s/m. All dimensions are in mm.

Since the examined obstacles are different both in terms of size and anatomy, the aforementioned dimensional values are not directly comparable. Thus, the aim of this paper is not to make a direct comparison between the dimensional values belonging to different category of obstacles (e.g. cylinder-like, emergent vegetation, and submerged vegetation). Otherwise, the obtained results could be misleading due to scale and size effects. Instead, only the dimensional values belonging to same group of obstacles were directly compared with each other. So as to compare the observed scour patterns with each other, in addition to these dimensional parameters, ratios between the geometrical characteristics of scour, i.e. P_t, P_s, P_f, V_R, and P_{tc}, are introduced in Table 3 and quantified in Table 2.

When S_w and S_d values in Table 2 and Figs. 5 - 8 are considered it can be stated that relatively wider and deeper scour holes occurred for the solid cylinder compared to HACC and vegetation cases under identical flow conditions. Also it can be seen from Fig. 6 that HACCs generated more elongated (i.e. less localized) scour holes compared to solid cylinder cases. The higher S_a values for the HACC in Table 2 confirm this assertion. A distinguishing feature of the HACC scour pattern is the formation of a sharp ridge at the downstream. Since the formations of sharp ridges were also detected in all the examined vegetative elements it can be stated that HACC represents trunky isolated vegetative elements more realistically compared to a rigid cylinder in terms of

Table 3: Definition of the morphometric parameters

Morphometric Parameter	Remarks
$P_t = \dfrac{S_v}{S_a}$	P_t is the ratio of scour volume to scour area and it has length dimensions. In other words, P_t gives the equivalent prismatic scour depth over the scoured area. This parameter quantifies the distribution of the erosive impact of the obstacle over the scoured area.
$P_s = \dfrac{S_d}{d_{VERC}}$	P_s describes the scour depth that occurs for the unit diameter of the VERC. Thus P_s corresponds to the conventional S/D parameter which is commonly used for the scour around rigid cylinder studies [55].
$P_f = \dfrac{S_v}{S_w^3}$	The form factor P_f is the scour volume over cube of scour width and characterizes the form of the scour volume. Its value increases with the increasing value of scour volume for a given scour width. Alternatively, the value of P_f increases with the decreasing value of scour width for a given scour volume. From this perspective it can be stated that the form factor P_f quantifies the locality of the scour volume. Lower values of P_f in a way indicate that the scour is distributed over a narrow area rather than a wide region.
$V_R = \dfrac{D_v}{S_v}$	The examination of the deposition pattern behind the obstacle can provide valuable information about the deposition structure [46]. From this motivation it was assumed that it has a certain significance to quantify how much scoured volume is deposited within the monitoring zone. To clarify this question, dimensionless volumetric deposition ratio V_R was introduced.
$P_{tc} = \dfrac{S_{ac}}{S_{lc}}$	P_{tc} quantifies the prismatic equivalent scour depth over the centerline and its meaning resembles P_t. Fig. 9 is the definition sketch which explains the relevant variables. However, differing from the P_t, P_{tc} presents two-dimensional analysis of the scour hole along the centerline. With the increasing value of P_{tc} the scour area increases over the length where the scour is monitored along the centerline.

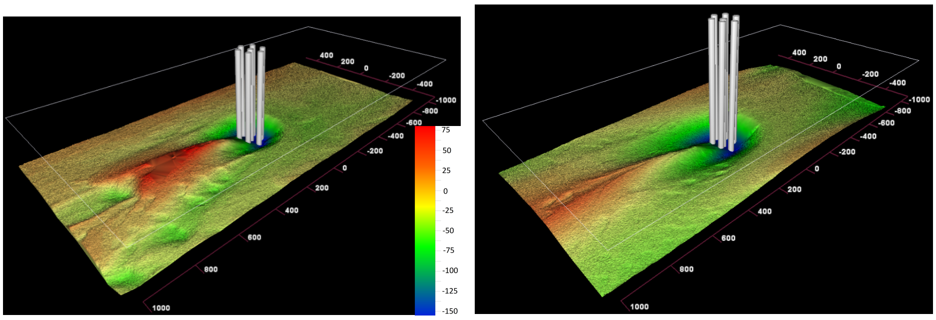

(a) (b)

Figure 6: Scour patterns for (a) emergent cylinder for 59 l/s/m, (b) emergent cylinder for 85 l/s/m, (c) HACC for 59 l/s/m, and (d) HACC for 85 l/s/m. All dimensions are in mm and the obstacles are scaled.

scouring process. For emergent vegetation (Fig. 7), the scour area expands at the downstream and this becomes more notable when the plant is bended. This is owed to the subcanopy flow, which creates a highly erosive jet in the plant vicinity. Similar findings were reported by Hill et al. [79], who investigated the scour pattern around an axial-flow hydrokinetic turbine model. The presence of the turbine leads to flow contraction between the bottom tip and the movable bed, and as a result the flow accelerates and local shear stress increases. Finally, they showed that the induced subcanopy jet is the main scouring mechanism by comparing the obtained scour pattern with the one generated from the turbine support tower only.

According to Table 2 the values of S_v are at the same order of magnitude for solid cylinder and emergent vegetation, despite the fact that d_{VERC} of the plant is approximately five times lower than that of the solid cylinder. This implies that the form of emergent vegetation is considerably more erosive. On the other hand, the deposition height is significantly lower for emergent vegetation. Moreover, with the effect of bending, while the projected area decreases (Table 2) the bulk volume slightly increases (Fig. 4b) in general. Consequently, S_d, S_v and S_w values markedly decrease compared to that of intact emergent case of the same plant. The artificially impermeable cases for both emergent and submerged vegetation cases generated deeper scour holes compared to their natural counterparts, despite the fact that the projected area (Table 2) and bulk submerged volume (Fig. 4b) decreased considerably. The scour patterns in Figs. 7 and 8

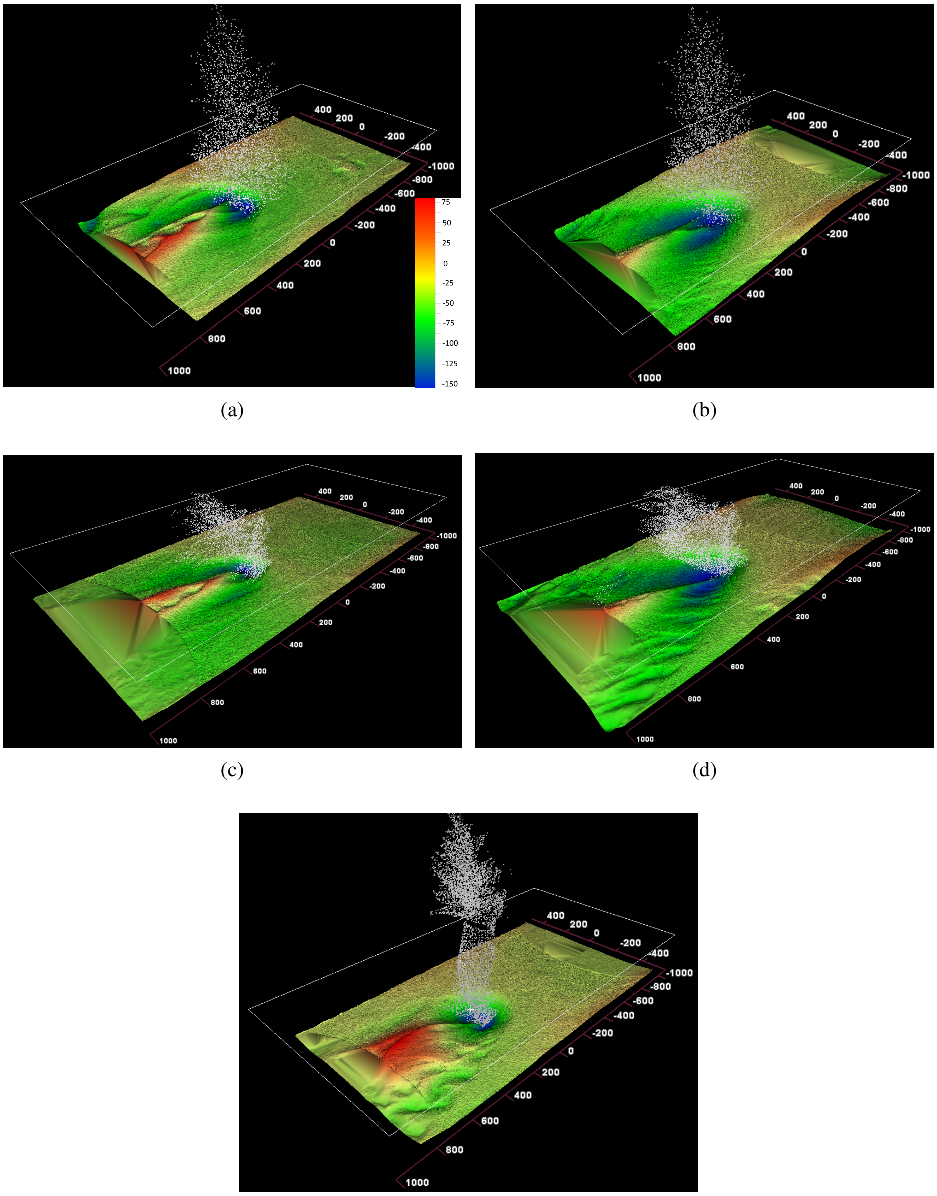

(a) (b)

(c) (d)

(e)

Figure 7: Scour patterns for (a) intact emergent vegetation for 59 l/s/m, (b) intact emergent vegetation for 85 l/s/m, (c) bended emergent vegetation for 59 l/s/m, (d) bended emergent vegetation for 85 l/s/m, and (e) impermeable emergent vegetation for 59 l/s/m. All dimensions are in mm and the obstacles are scaled.

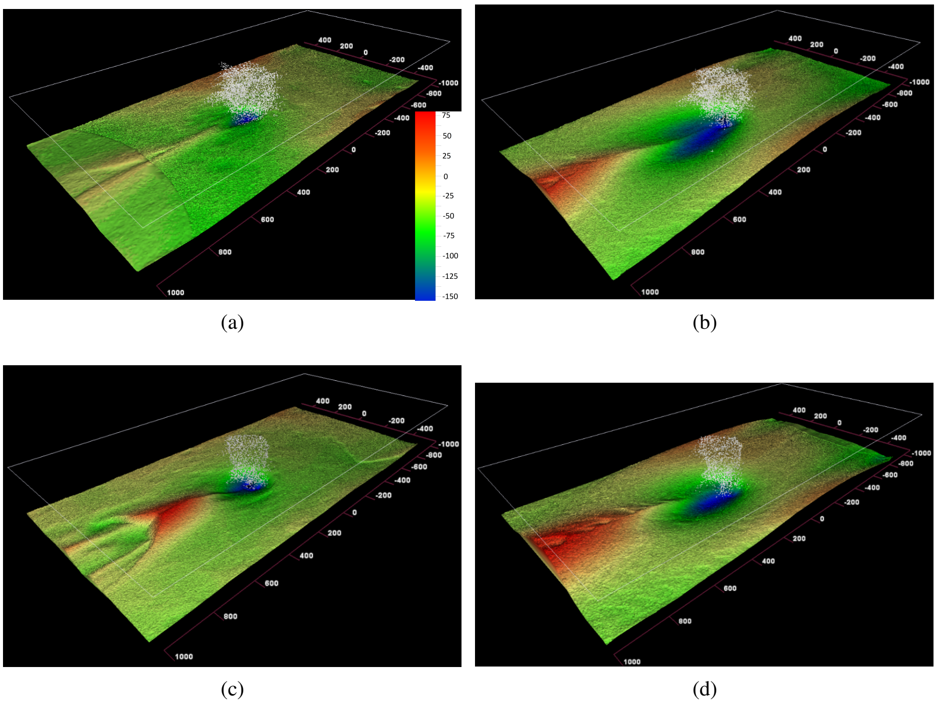

Figure 8: Scour patterns for (a) intact submerged vegetation for 59 l/s/m, (b) intact submerged vegetation for 85 l/s/m, (c) impermeable submerged vegetation for 59 l/s/m, and (d) impermeable submerged vegetation for 85 l/s/m. All dimensions are in mm and the obstacles are scaled.

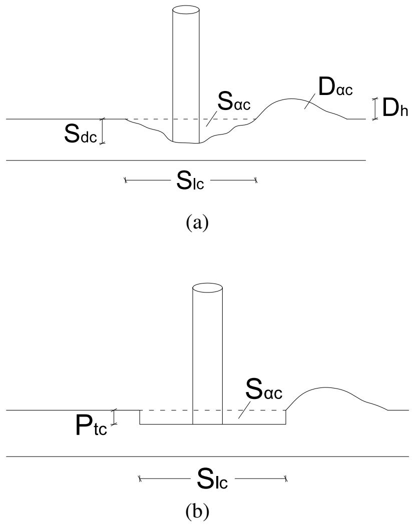

Figure 9: Depiction of the variables denoting the scour pattern characteristics for (a) the actual scour pattern and (b) the equivalent uniform scour hole.

also demonstrated that scour becomes localized for the impermeable cases for both emergent and submerged plants. S_d values in Table 2 indicate that while the scour depth is less for emergent vegetation compared to that of the impermeable version, scour area and scour volume is more for intact emergent vegetation compared to impermeable case. This implies that when vegetation is rendered impermeable, scouring becomes localized, in a narrower region, with a higher scour depth similar to the solid cylinder case.

As can be concluded from Table 2, emergent vegetation and its impermeable version generate close P_t values to each other, pointing out the similarity of their erosive effects within the scoured area. The values in Table 2, also reveal that when emergent vegetation is bended, the value of P_t decreases. Under the influence of bending, the plant takes a more streamlined form (in spite of the fact that its bulk submerged volume increases, albeit slightly, according to Fig. 4b), which leads to a decreased prismatic scour depth within the scoured area. Not only the decreased value of P_t but also the decreased values of S_d, S_v, and S_w further confirm this idea. P_t values in Table 2 also showed that HACC has considerably less erosive impact compared to the solid cylinder due to its permeable nature.

Observed higher values of P_f for vegetative elements compared to other obstacles in Fig. 10(a) confirm that all the permeable forms of vegetative elements bring about similar scouring patterns, which are distributed over a larger area compared to the impermeable versions of the vegetative elements, solid cylinder, and HACC cases. In Fig. 10(b), the variation of P_s versus Reynolds number is presented. As can be inferred from Fig. 10(b), the permeable forms of vegetative elements have higher P_s values compared to impermeable forms of the obstacles. The variation of θ/θ_{cr} versus P_s, which is given in Fig. 11(a), also showed in a similar way that permeable forms of the plants generate at least 2-4 times higher values of P_s under the same flow conditions, which emphasizes the erosive influence of the vegetative elements compared to other impermeable forms. Another common interesting point in Figs. 10(a), 10(b), and 11(a) is that the permeable forms of the plants react in a much more variable way compared to other types of obstacles. This implies that there is a higher sensitivity to flow conditions (either described by Reynolds or Shields number). More specifically natural vegetation reacts to flow in a more variable way compared to the other examined obstacles. This can be explained by the streamlining and compression behavior of the plant. According to Yagci et al. [44] vegetation with distinct trunk exhibits three different forms (i.e. erect, compressed, and bended) under the impact of the flow induced drag force. In the compression, the branches and foliages follow the streamlines, and the permeability of the vegetation decreases.

The variation of θ/θ_{cr} with respect to V_R (Fig. 11b) clearly demonstrated that, for the higher discharges, the deposited volume ratio within the monitoring zone decreases for all the obstacles without any exception. Also the V_R values given in Table 2 showed that the vegetative elements yield less deposition ratio compared to cylinder-like obstacles within the monitoring zone under the same flow conditions. Moreover, impermeable forms of the obstacles are prone to generate more deposition within the monitoring zone compared to permeable forms of the obstacles. As can be seen from Fig. 10(c), even for small Reynolds number, the permeable form of both submerged and emergent vegetation generates highly elevated values of P_{tc}. The HACC, which generated similar scour pattern to vegetation type obstacles, constitutes a transition case between permeable vegetation type of obstacles and impermeable form of the obstacles. Im-

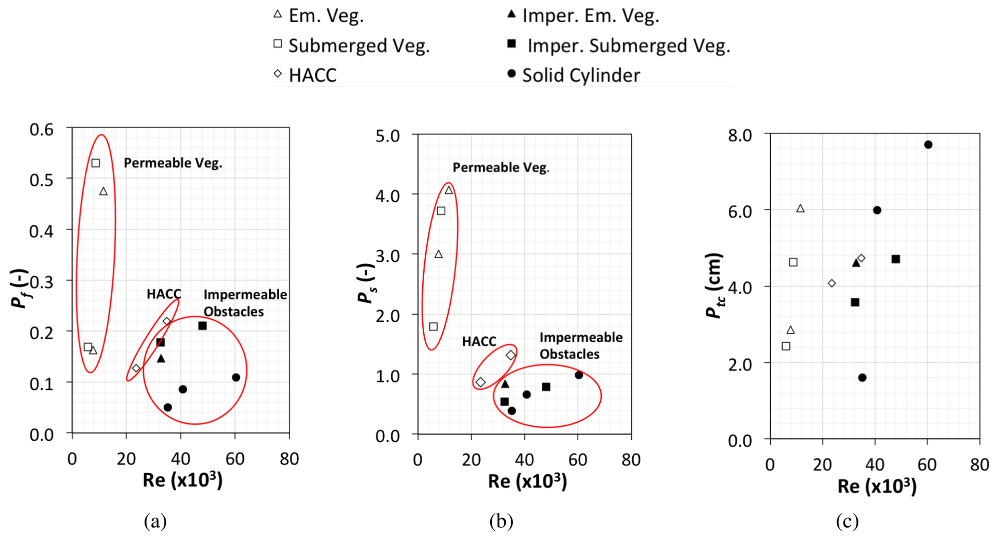

Figure 10: Variation of the parameters (a) P_f, (b) P_s, and (c) P_{tc} with Reynolds number

permeable form of the obstacles (both vegetation-type and cylinder-like) requires significantly higher (according to Fig. 10c, approximately 3-4 times) Reynolds number for the generation of same magnitude of P_{tc} within the scoured zone along the centerline.

Fig. 12 shows the longitudinal centerline profiles of the scoured bed under seven different types of obstructions for the low and high discharge (i.e. 13 of the 14 tests given in Table 2). According to Fig. 12, the upstream slopes of the scour holes are practically parallel to each other for all the obstacles. The values of J_{ups} and J_{side} presented in Table 2 also numerically confirm that scour angles at the upstream and at the side are around the same magnitude for all the forms of the obstacles but the submerged vegetation types. The slopes of the scour holes are significantly less compared to other cases for the submerged plants. As can be seen from Fig. 12, the downstream slope of both the emergent and submerged vegetation is milder compared to cylinder-like cases. Fig. 12 also shows that the maximum scour depth for all the obstacles is located at the upstream of the obstacle as expected [54]. The patterns of the scour for the cylinder cases look similar to the description given in [55], with relatively steeper scour angle upstream and milder downstream. Same patterns were also monitored for all the vegetative elements.

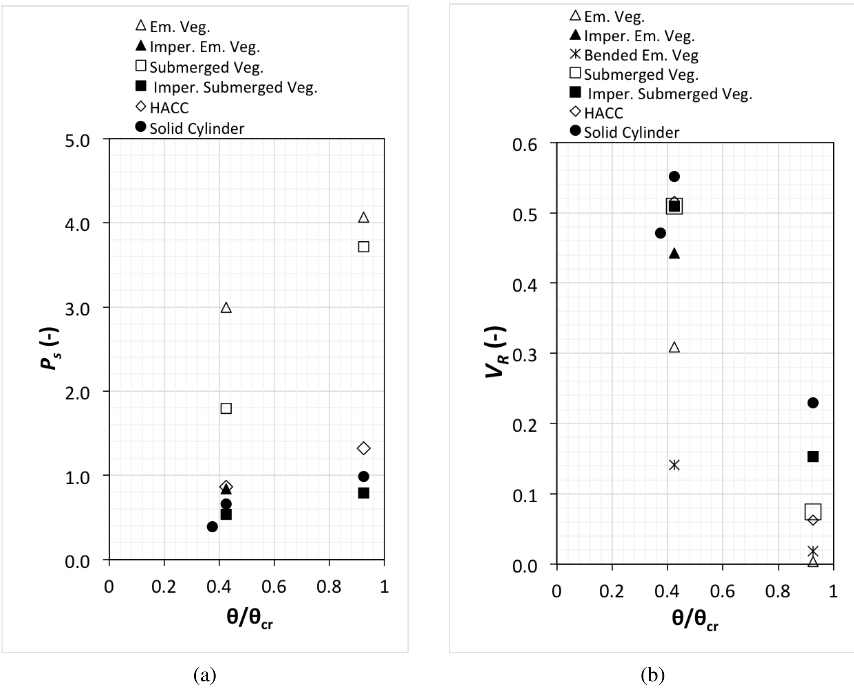

Figure 11: Variation of the parameters (a) P_s and (b) V_R with θ/θ_{cr}

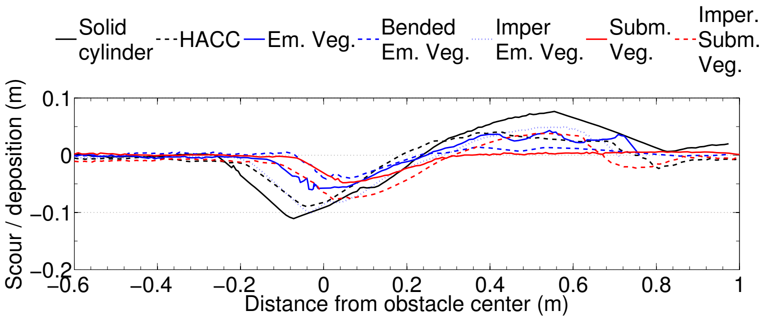

(a)

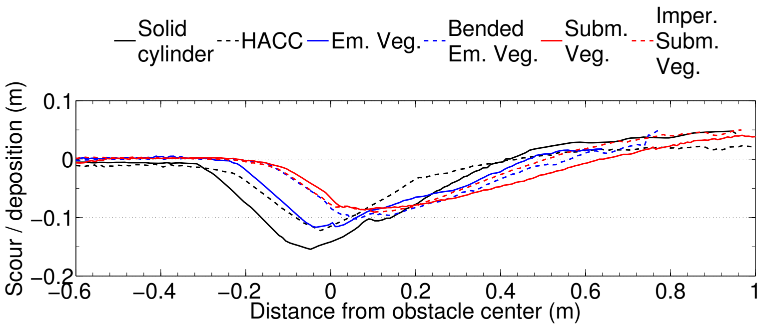

(b)

Figure 12: Longitudinal scour profiles along the flume centerline for (a) 59 l/s/m and (b) 85 l/s/m.

4.2. Hydrodynamic analysis of the scour/deposition patterns

4.2.1. Solid cylinder and hexagonal array of circular cylinders

Sumer [57] summarized the consequences of placing a structure in a hydraulic environment and the alterations of the flow pattern around it: contraction of the flow, downflow occurrence at the upstream of the structure, formation of a horseshoe vortex, formation of lee-wake vortices (with or without vortex shedding), and increased turbulence in the vicinity of the structure. The scouring is more pronounced with increasing flow velocity since the sediment mobility increases (see Shields parameter values in Table 1). Fig. 5 shows the generated scour patterns around the solid cylinders, which is similar to those of [53–55, 71]. For the higher discharge, the peak point of the depositional zone is not observed within the monitoring zone.

Fig. 6 shows the scanned bed for the cylinder array (HACC) cases. The structure has the same outer diameter with the previous solid cylinder case; however, its permeability apparently plays a role in the generation of different scour patterns. It is a well-documented fact [46, 80] that since the array has a specific porosity, certain amount of flow penetrates through the array as bleed-flow. Zong and Nepf [80] visualized the wake behind the porous obstruction and concluded that the presence of the bleed-flow delays the onset of the von Karman vortex street compared to the solid cylinder case.

Recently, Kitsikoudis et al. [81] experimentally investigated the flow characteristics around different forms of HACC cylinders, which have equal encircling diameter with this study. In their study Kitsikoudis et al. [81] mounted the obstacles on rigid bottom and performed velocity measurements along the centerline and around the porous obstruction. Their data clearly showed the existence of the downflow at the upstream of the HACC, in spite of the presence of bleed-flow. They also found that with decreasing permeability, the downflow strength increased due to decreasing bleed-flow. This finding, as well as the appearance of the upstream part of the scour hole seen in Fig. 6, suggests that the downflow still plays a significant role in the scouring process, similarly to the solid cylinder in Fig. 5. Nevertheless, it should be noted that the extent of the upstream scour hole is significantly lower for HACC compared to solid cylinder (Fig. 6), as a result of the fact that the magnitude of the downflow is lessened for the HACC compared to solid

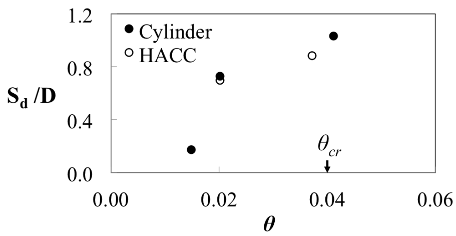

Figure 13: Non-dimensional scour depth (S/D) with the Shields parameter (θ) for the individual cylinder and the HACC cases

cylinder as proved by Kitsikoudis et al. [81]. According to Graf and Istiarto [54] the strength of the horseshoe vortex heavily depends on the downflow strength. Based on this knowledge it can be claimed that with the reduced downflow, the upstream separation distance near the bottom is diminished, which is the natural outcome of the downflow. Consequently, the magnitude of the horseshoe vortex is lessened as a result of decreased downflow. Therefore, the spanwise extents of the scour holes S_w for HACCs are smaller than the solid cylinders.

The aforementioned differences in the extent of scour hole between single cylinder and HACC cases can also be seen in the depth at the upstream part of the scour holes. Fig. 13 shows the variation of the non-dimensional scour depth (S_d/D) with the Shields parameter (θ) for the individual cylinder and the HACC cases (note that $S_d/D \neq P_s$ for HACC). D represents the outer diameter of the solid cylinder and HACC. On this figure, the critical value of Shields parameter for initiation of motion (with respect to modified Shields diagram of [82]) is also shown. Similar exercises were followed previously by Mao [83] and Melville and Coleman [84]. It can be seen that the non-dimensional scour depth values for the two cases are quite close for the smaller value of Shields parameter provided that the overall diameter of the HACC is taken as the representative diameter. However, as the Shields parameter increases towards the live-bed regime, the scour depths of HACC deviate from the solid cylinder case, albeit slightly. According to criteria given in [85, 86], the array of HACC employed here is considered to have a dense configuration, thus its behavior is closer to a rigid cylinder of equal total volume.

4.2.2. *Emergent vegetation case (intact, bended, and impermeable cases)*

4.2.2.1 Intact emergent vegetation

The flow field around emergent vegetation with distinct trunk can conceptually be classified into two specific regions; the canopy and subcanopy regions. Yagci et al. [44] obtained the mean flow and turbulence patterns at the centerline where flow passes through an emergent plant (*Cupressus Macrocarpa*, same species with the one used in this study), based on their spatially dense measurements for rigid bed case. Since those findings may considerably aid the explanation of the obtained scour patterns around the plants, their results are reproduced here, in Fig. 14. In [44], as can be seen from the streamwise component in Fig. 14, a strong subcanopy jet was observed just below the plant, which makes the flow around/through emergent tree-like vegetation unique in terms of flow-body interaction. The strength of the subcanopy flow heavily depends on the porosity and the ratio of plant submergence, i.e. trunk to canopy ratio. The experimental data by Kitsikoudis et al. [87] clearly demonstrated that the strength of the subcanopy flow decreases with the increasing porosity. Nevertheless, in the pertinent literature there is no systematic study which investigates the influence of trunk to canopy ratio on the characteristics of the subcanopy flow. In this study, these two parameters (i.e. porosity and trunk to canopy ratio) were kept constant for the plants. However, it should be noted that different scour patterns may be obtained for the different values of these parameters.

Recently, the experimental data by Kitsikoudis et al. [81] showed that flow recovery behind a tree-like element occurred in a shorter distance compared to the respective uniform element, due to the vertical shear induced turbulent mixing between subcanopy and canopy region. Moreover, it was seen that for the tree-like element configuration, the von Karman vortex street was distorted to a great extent, which was attributed to the interaction of the subcanopy jet with the lee-wake vortices that occur behind the canopy. These findings highlight that subcanopy dictates the flow field behind tree-like vegetation. The conical scour pattern occurs around the solid cylinder as a result of the horseshoe vortex, as can be seen in Fig. 5. However, differing from the solid cylinder case, horseshoe vortex is not the major coherent flow which is responsible for the scour around the tree-like element. Instead, subcanopy flow dictates the scouring mechanism around

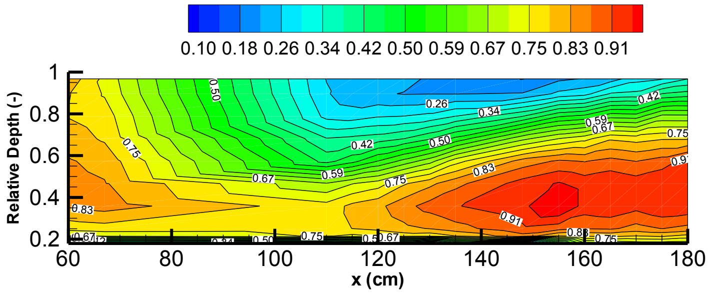

(a)

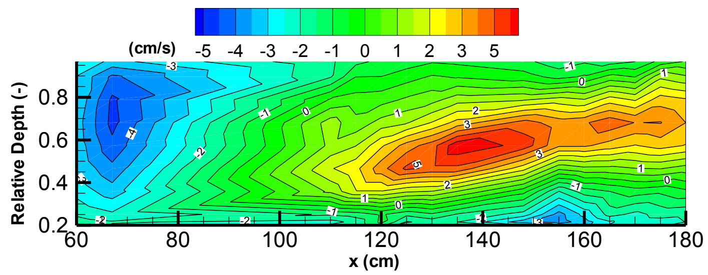

(b)

Figure 14: Time-averaged velocity contour plots at the downstream of an emergent vegetal element (*Cupressus Macrocarpa* species). The plant is located at x=82 cm. (a) The contours of the dimensionless streamwise time-averaged mean velocity (U/U_{max}) and (b) the vertical time-averaged mean velocity contours. Obtained from Yagci et al. [44].

the vegetation. The subcanopy jet seems to be the probable reason that creates the relative milder downstream scour slope, which was described in previous section. Moreover, Fig. 14 proves the existence of a downflow for emergent vegetation, similar to the case of solid cylinder. The scour patterns in Fig. 7 suggest that the downflow affects the scouring process for the plants, similarly to solid cylinder and HACC cases, given that noticeable scour was observed at the upstream of the trunk.

4.2.2.2 *Impermeable emergent vegetation*

Impermeable emergent vegetation generated significantly higher volumetric deposition ratio V_R values compared to intact emergent vegetation within the monitoring zone. This means that with decreasing permeability the deposition occurs closer to the obstacle.

4.2.2.3 Bended emergent vegetation

According to Lightbody and Nepf [88], when salt marsh vegetation bends under the effect of drag force for a given depth the vertical variation in the projected area of the element is negligible. However, the projected area values in Table 2 clearly demonstrated that despite the plant is artificially bended, the projected area decreases for bended trunky vegetation. On the other hand, with the effect of bending the submerged bulk volume of the plant increases (Fig. 4a). Jarvela [89] documented that leaves on willows can double or triple the friction factor compared to the leafless case. This was later on further confirmed by Wilson et al. [90] who reported that plant foliage induces larger drag forces. This implies that when vegetal obstruction bends and compresses under the effect of flow, its submerged volume increases, hence one would expect the total drag also to increase. However, with the increasing bending, according to Righetti [91], vegetation gains a more hydrodynamic shape and streamlining effect becomes more prominent. Moreover, recently Majd et al. [92] conducted flow visualization and quantified the separation (which is the natural outcome of downflow according to Graf and Istiarto [54]) at the upstream of the bended cylinder by means of a laser sheet. They found that the upstream separation distance tends to decrease with the bending of the cylinder. These offsetting factors (i.e. increased plant volume and better developed hydrodynamic shape of the plant) have opposite effects on the generated drag force.

When all these pieces are put together, it can be reasoned that with the increasing immersed volume and decreased permeability, the magnitude of the downflow would increase. On the other hand, with the increasing hydrodynamic shape owing to bending, increased portion of the flow is expected to be diverted upwards. This mitigates the magnitude of downflow and reduces the strength of subcanopy flow.

According to Table 2, with the effect of bending, the values of S_d, S_v and S_w markedly decrease compared to that of intact emergent case. This advocates that under the same flow conditions, the hydrodynamic influence of bending prevails over the decreased porosity and increased submerged volume. This mitigates the magnitude of the downflow. This result is also in agreement with the findings of Fathi-Maghadam and Kouwen [93], who showed that the standard drag force equation becomes invalid for flexible trees owing to the bending and compression of the plant. In their study, the drag force unexpectedly correlates linearly with the velocity (instead of the regular correlation with the square of the velocity), which confirms that bending/compression substantially reduces the drag force. It is worth to mention that this study was conducted in unconfined flow (i.e. air) domain by towing the vegetation. Moreover, in parallel with the findings presented here, the findings by Euler et al. [48] demonstrated that the streamwise inclination reduces the horseshoe vortex stresses acting at the projected frontal area, which leads to a reduction of frontal scouring around solitary woody riparian plants.

4.2.2.4 Submerged vegetation

Fig. 8 shows the scour patterns obtained from the experimental runs with intact and with impermeable canopy submerged vegetation. As stated in Section 4.1, both upstream-slope of scour holes J_{ups} and side-slope of scour holes J_{side} are markedly lower for submerged vegetation compared to other obstacles. The most distinguished difference between the flow through/around emergent vegetation and flow through/around submerged vegetation is the presence of over-canopy flow, which occurs only for the submerged case of the plant. The scouring mechanism is similar to the emergent vegetation; however, the downflow is now expected to be diminished due to the fact that a portion of the flow passes over the plant. Nonetheless, additional studies are needed to clarify the role of over-canopy flow on the reduction of downflow and scour.

5. Conclusions

In riverine systems, riparian vegetation plays a crucial role in the regeneration of river landscapes by altering fluvial as well as biological processes. A better understanding of dynamic interaction between the flow, vegetation, and sediment processes would aid in the development of sustainable river management strategies. From this motivation, an experimental study was undertaken which focused on the scour/deposition geometry around some representative vegetation elements. The following conclusions were drawn based on the findings:

- Dimensionless morphometric values demonstrated that a solid cylinder generated relatively wider and deeper scour holes compared to a hexagonal array of circular cylinders (HACC) and vegetation cases under identical flow conditions. While the cylinder produced a pronounced circular extent of the scour hole, the natural plant generated two elongated scour holes at the downstream with a well-defined longitudinal ridge. The HACC case can be considered as a transitional form between a plant and a cylinder. Similar to the real plant cases, an elongated scour hole and a well-defined ridge could clearly be distinguished. From this perspective it can concluded that HACC represents complex vegetation anatomy in a more successful way in terms of local scouring impact on erodible bed.

- Differing from the solid cylinder, a strong subcanopy jet and the bleed-flow are known to be the characteristic features that make the flow around/through tree-like emergent vegetation unique in terms of flow-body interaction. For the examined cases, in spite of the fact that d_{VERC} of tree-like emergent vegetation is approximately five times lower than that of the solid cylinder, due to the presence of subcanopy flow scour volumes of solid cylinder and emergent vegetation are at a comparable level. Moreover, subcanopy flow leads to significant scour expansion at the downstream of the emergent vegetation, contrary to the cylinder and HACC cases.

- When the emergent plant was modified as an impermeable obstacle, it was seen that the distance between the obstacle and the deposition region at the downstream became shorter. Furthermore, an elongated scour pattern and the ridge were not observed for the impermeable case.

- When natural vegetation becomes artificially impermeable scouring becomes localized. It occurs in a narrower region with higher scour depth, as observed for the solid cylinder case.

- When the emergent vegetation was bended, the plant takes more streamlined form despite its increasing bulk submerged volume. The values of scour depth, scour volume, and scour width considerably decrease compared to that of intact emergent case. The scour zone at downstream became more elongated and expanded compared to the intact vegetation case.

- Within the monitoring zone, plants generate less dimensionless volumetric deposition ratio V_R compared to cylinder-like obstacles. Similarly, impermeable forms of vegetation tend to generate higher V_R within the monitoring zone compared to their permeable counterparts.
- The data showed that the upstream slopes of the scour holes are practically equal to each other for all the obstacles except submerged vegetation. The downstream slopes of both emergent and submerged vegetation are milder compared to cylinder-like cases.
- The obtained morphometric scour characteristics belonging to natural vegetation clearly demonstrated that such plants exhibit higher sensitivity to the incoming flow. In other words, the plant form changes (due to streamlining and compression effect) when exposed to flow. Thus it yields more variable morphometric scour characteristics compared to other rigid obstacles.

Acknowledgements

The financial support provided to Vasileios Kitsikoudis from Anastasios Anastasiadis foundation (grant number 63310/25-09-2013) for the first part of this study and the Scientific and Technological Research Council of Turkey (TUBITAK) - Fellowship Program 2216 (Ref. No. 21514107-115.02-45898) for post-doctoral research in Istanbul Technical University for the final part of this study is gratefully acknowledged. Manousos Valyrakis acknowledges the support of the Royal Society (Research Grant RG2015 R1 68793/1) and the Royal Society of Edinburg (Crucible Award). The authors thank the anonymous Reviewers for their constructive comments.

[1] H. M. Nepf, Hydrodynamics of vegetated channels, J. Hydraul. Res. 50 (3) (2012) 262–279. doi:10.1080/00221686.2012.696559.

[2] J. C. Curran, W. C. Hession, Vegetative impacts on hydraulics and sediment processes across the fluvial system, J. Hydrol. 505 (2013) 364–376. doi:10.1016/j.jhydrol.2013.10.013.

[3] A. Gurnell, Plants as river system engineers, Earth Surf. Process. Landf. 39 (2014) 4–25. doi:10.1002/esp.3397.

[4] E. Istanbulluoglu, R. L. Bras, Vegetation-modulated landscape evolution: Effects of vegetation on landscape processes, drainage density, and topography, J. Geophys. Res. 110 (F2) (2005) F02012. doi:10.1029/2004JF000249.

[5] A. B. Murray, M. A. F. Knaapen, M. Tal, M. L. Kirwan, Biomorphodynamics: Physical-biological feedbacks that shape landscapes, Water Resour. Res. 44 (11) (2008) W11301. doi:10.1029/2007WR006410.

[6] W. Vandenbruwaene, S. Temmerman, T. J. Bouma, P. C. Klaassen, M. B. de Vries, D. P. Callaghan, P. van Steeg, F. Dekker, L. A. van Duren, E. Martini, T. Balke, G. Biermans, J. Schoelynck, P. Meire, Flow interaction with dynamic vegetation patches: Implications for biogeomorphic evolution of a tidal landscape, J. Geophys. Res. 116 (F1) (2011) F01008. doi:10.1029/2010JF001788.

[7] H. M. Gibbs, A. M. Gurnell, C. M. Heppell, K. L. Spencer, The role of vegetation in the retention of fine sediment and associated metal contaminants in London's rivers, Earth Surf. Process. Landf. 39 (2014) 1115–1127. doi:10.1002/esp.3575.

[8] S. V. Gregory, F. J. Swanson, W. A. McKee, K. W. Cummins, An ecosystem perspective of riparian zones, BioScience 41 (8) (1991) 540–551. doi:10.2307/1311607.

[9] K. Sand-Jensen, T. Vindbaek Madsen, Patch dynamics of the stream macrophyte, Callitriche cophocarpa, Freshwater Biol. 27 (2) (1992) 277–282. doi:10.1111/j.1365-2427.1992.tb00539.x.

[10] R. J. Wilcock, P. D. Champion, J. W. Nagels, G. F. Croker, The influence of aquatic macrophytes on the hydraulic and physico-chemical properties of a New Zealand lowland stream, Hydrobiologia 416 (1999) 203–214. doi:10.1023/A:1003837231848.

[11] M. Schulz, H.-P. Kozerski, T. Pluntke, K. Rinke, The influence of macrophytes on sedimentation and nutrient retention in the lower River Spree (Germany), Water Res. 37 (3) (2003) 569–578. doi:10.1016/S0043-1354(02)00276-2.

[12] A. Gurnell, J. M. O'Hare, M. T. O'Hare, M. J. Dunbar, P. M. Scarlett, An exploration of associations between assemblages of aquatic plant morphotypes and channel geomorphological properties within British rivers, Geomorphology 116 (1-2) (2010) 135–144. doi:10.1016/j.geomorph.2009.10.014.

[13] D. Termini, Effect of vegetation on fluvial erosion processes: Experimental analysis in a laboratory flume, Procedia Environ. Sci. 19 (2013) 904–911. doi:10.1016/j.proenv.2013.06.100.

[14] B. Doulatyari, S. Basso, M. Schirmer, G. Botter, River flow regimes and vegetation dynamics along a river transect, Adv. Water Resour. 73 (2014) 30–43. doi:10.1016/j.advwatres.2014.06.015.

[15] H. P. Rauch, Hydraulic impact of a vegetated river bank exemplified by the soil bioengineering test flume of the river Wien, Ph.D. thesis, Institute of Soil Bioengineering and Landscape Construction, University of Natural Resources and Applied Life Sciences, Vienna, Austria (2005).

[16] W. Bertoldi, A. Siviglia, S. Tettamanti, M. Toffolon, D. Vetsch, S. Francalanci, Modeling vegetation controls on fluvial morphological trajectories, Geophys. Res. Lett. 41 (20) (2014) 7167–7175. doi:10.1002/2014GL061666.

[17] Y. P. Dhital, Q. Tang, Soil bioengineering application for flood hazard minimization in the foothills of Siwaliks, Nepal, Ecol. Eng. 74 (2015) 458–462. doi:10.1016/j.ecoleng.2014.11.020.

[18] M. Tal, C. Paola, Dynamic single-thread channels maintained by the interaction of flow and vegetation, Geology

35 (4) (2007) 347–350. doi:10.1130/G23260A.1.

[19] A. M. Gurnell, W. Bertoldi, D. Corenblit, Changing river channels: The roles of hydrological processes, plants and pioneer fluvial landforms in humid temperate, mixed load, gravel bed rivers, Earth-Sci. Rev. 111 (1-2) (2012) 129–141. doi:10.1016/j.earscirev.2011.11.005.

[20] L. B. Leopold, T. Maddock, The Hydraulic Geometry of Stream Channels and Some Physiographic Implications, Geological Survey Professional Paper 252, United States Goverment Printing Office, Washington DC, 1953.

[21] D. L. Rosgen, A classification of natural rivers, CATENA 22 (3) (1994) 169–199. doi:10.1016/0341-8162(94)90001-9.

[22] S. Ikeda, N. Izumi, Width and depth of self-formed straight gravel rivers with bank vegetation, Water Resour. Res. 26 (10) (1990) 2353–2364. doi:10.1029/WR026i010p02353.

[23] R. G. Millar, M. C. Quick, Effect of bank stability on geometry of gravel rivers, J. Hydraul. Eng. 119 (12) (1993) 1343–1363. doi:10.1061/(ASCE)0733-9429(1993)119:12(1343).

[24] D. R. Montgomery, Geomorphology, river ecology, and ecosystem management, in: J. M. Dorava, D. R. Montgomery, B. B. Palcsak, F. A. Fitzpatrick (Eds.), Geomorphic Processes and Riverine Habitat, American Geophysical Union, Washington D.C., 2001, pp. 247–253.

[25] T. Tsujimoto, Fluvial processes in streams with vegetation, J. Hydraul. Res. 37 (6) (1999) 789–803. doi:10.1080/00221689909498512.

[26] G. J. Brierly, K. A. Fryirs, Geomorphology and River Management, Blackwell Publishing, 2005.

[27] F. Carollo, V. Ferro, D. Termini, Flow velocity measurements in vegetated channels, J. Hydraul. Eng. 128 (7) (2002) 664–673. doi:10.1061/(ASCE)0733-9429(2002)128:7(664).

[28] M. Righetti, A. Armanini, Flow resistance in open channel flows with sparsely distributed bushes, J. Hydrol. 269 (1-2) (2002) 55–64. doi:10.1016/S0022-1694(02)00194-4.

[29] F. G. Carollo, V. Ferro, D. Termini, Flow resistance law in channels with flexible submerged vegetation, J. Hydraul. Eng. 131 (7) (2005) 554–564. doi:10.1061/(ASCE)0733-9429(2005)131:7(554).

[30] E. Kubrak, J. Kubrak, P. M. Rowinski, Vertical velocity distributions through and above submerged, flexible vegetation, Hydrol. Sci. J. 53 (4) (2008) 905–920. doi:10.1623/hysj.53.4.905.

[31] W. X. Huaia, Y. H. Zenga, Z. G. Xub, Z. H. Yang, Three-layer model for vertical velocity distribution in open channel flow with submerged rigid vegetation, Adv. Water Resour. 32 (4) (2009) 487–492. doi:10.1016/j.advwatres.2008.11.014.

[32] M. Luhar, J. Rominger, H. Nepf, Interaction between flow, transport and vegetation spatial structure, Environ. Fluid Mech. 8 (5-6) (2008) 423–439. doi:10.1007/s10652-008-9080-9.

[33] F. Jahra, Y. Kawahara, F. Hasegawa, H. Yamamoto, Flow-vegetation interaction in a compound open channel with emergent vegetation, Intl. J. River Basin Manag. 9 (3-4) (2011) 247–256. doi:10.1080/15715124.2011.642379.

[34] I. Nezu, K. Onitsuka, Turbulent structures in partly vegetated open-channel flows with LDA and PIV measurements, J. Hydraul. Res. 39 (6) (2001) 629–642. doi:10.1080/00221686.2001.9628292.

[35] C. A. M. E. Wilson, O. Yagci, H.-P. Rauch, N. R. B. Olsen, 3D numerical modelling of a willow vegetated river/floodplain system, J. Hydrol. 327 (1-2) (2006) 13–21. doi:10.1016/j.jhydrol.2005.11.027.

[36] C. A. M. E. Wilson, O. Yagci, H.-P. Rauch, T. Stoesser, Application of the drag force approach to model the flow?interaction of natural vegetation, Intl. J. River Basin Manag. 4 (2) (2006) 137–146. doi:10.1080/15715124.2006.9635283.

[37] M. McBride, W. C. Hession, D. M. Rizzo, D. M. Thompson, The influence of riparian vegetation on near-bank turbulence: a flume experiment, Earth Surf. Process. Landf. 32 (13) (2007) 2019–2037. doi:10.1002/esp.1513.

[38] A. N. Sukhodolov, I. Schnauder, W. S. J. Uijttewaal, Dynamics of shallow lateral shear layers: Experimental study in a river with a sandy bed, Water Resour. Res. 46 (11) (2010) W11519. doi:10.1029/2010WR009245.

[39] A. C. Ortiz, A. Ashton, H. Nepf, Mean and turbulent velocity fields near rigid and flexible plants and the implications for deposition, J. Geophys. Res. 118 (4) (2013) 2585–2599. doi:10.1002/2013JF002858.

[40] C. Le Bouteiller, J. G. Venditti, Vegetation-driven morphodynamic adjustments of a sand bed, Geophys. Res. Lett. 41 (2014) 3876–3883. doi:10.1002/2014GL060155.

[41] E. M. Yager, M. W. Schmeeckle, The influence of vegetation on turbulence and bed load transport, J. Geophys. Res. 118 (3) (2013) 1585–1601. doi:10.1002/jgrf.20085.

[42] D. C. Le Maitre, D. F. Scott, C. Colvin, A review of information on interactions between vegetation and groundwater, Water SA 25 (2) (1999) 137–152.

[43] O. Yagci, M. S. Kabdasli, The impact of single natural vegetation elements on flow characteristics, Hydrol. Process. 22 (21) (2008) 4310–4321. doi:10.1002/hyp.7018.

[44] O. Yagci, U. Tschiesche, M. S. Kabdasli, The role of different forms of natural riparian vegetation on turbulence and kinetic energy characteristics, Adv. Water Resour. 33 (5) (2010) 601–614. doi:10.1016/j.advwatres.2010.03.008.

[45] D. W. S. A. Meire, J. M. Kondziolka, H. M. Nepf, Interaction between neighboring vegetation patches: Impact on flow and deposition, Water Resour. Res. 50 (5) (2014) 3809–3825. doi:10.1002/2013WR015070.

[46] S. C. Chen, H. C. Chan, Y. H. Li, Observations on flow and local scour around submerged flexible vegetation, Adv. Water Resour. 43 (2012) 28–37. doi:10.1016/j.advwatres.2012.03.017.

[47] I. Schnauder, H. L. Moggridge, Vegetation and hydraulic-morphological interactions at the individual plant, patch and channel scale, Aquat. Sci. 71 (3) (2009) 318–330. doi:10.1007/s00027-009-9202-6.

[48] T. Euler, J. Zemke, S. Rodrigues, J. Herget, Influence of inclination and permeability of solitary woody riparian plants on local hydraulic and sedimentary processes, Hydrol. Process. 28 (3) (2014) 1358–1371. doi:10.1002/hyp.9655.

[49] T. A. McMahon, The mechanical design of trees, Sci. Am. 233 (1) (1975) 92–102.

[50] T. A. McMahon, R. E. Kronauer, Tree structures: Deducing the principle of mechanical design, J. Theor. Biol. 59 (2) (1976) 443–466. doi:10.1016/0022-5193(76)90182-X.

[51] F. J. Sutili, L. Denardi, M. A. Durlo, H. P. Rauch, C. Weissteiner, Flexural behaviour of selected riparian plants under static load, Ecol. Eng. 43 (2012) 85–90. doi:10.1016/j.ecoleng.2012.02.012.

[52] R. H. J. Sellin, D. P. van Beesten, Conveyance of a managed vegetated two-stage river channel, Proc. ICE Water Manag. 157 (1) (2004) 21–33. doi:10.1680/wama.2004.157.1.21.

[53] B. Dargahi, Controlling mechanism of local scouring, J. Hydraul. Eng. 116 (10) (1990) 1197–1214. doi:10.1061/(ASCE)0733-9429(1990)116:10(1197).

[54] W. H. Graf, I. Istiarto, Flow pattern in the scour hole around a cylinder, J. Hydraul. Res. 40 (1) (2002) 13–20. doi:10.1080/00221680209499869.

[55] B. M. Sumer, J. Fredsoe, The Mechanics of Scour in the Marine Environment, Vol. 17 of Advanced Series on Ocean Engineering, World Scientific, 2002.

[56] A. Roulund, B. M. Sumer, J. Fredsoe, J. Michelsen, Numerical and experimental investigation of flow and scour around a circular pile, J. Fluid Mech. 534 (2005) 351–401. doi:10.1017/S0022112005004507.

[57] B. M. Sumer, Mathematical modeling of scour: A review, J. Hydraul. Res. 45 (6) (2007) 723–735. doi:10.1080/00221686.2007.9521811.

[58] M. Valyrakis, V. Kitsikoudis, O. Yagci, V. S. O. Kirca, E. Koursari, Experimental investigation of the modification of the flow field, past emergent aquatic vegetation elements, for distinct bed roughness, in: Submitted for review in the 36th IAHR World Congress, The Hague, The Netherlands, 2015.

[59] K. J. Gregory, D. E. Walling, Drainage basin form and process, Edward Arnold, London, 1973.

[60] E. J. Hickin, Vegetation and river channel dynamics, Can. Geogr. 28 (2) (1984) 111–126. doi:10.1111/j.1541-0064.1984.tb00779.x.

[61] I. Schnauder, O. Yagci, M. S. Kabdasli, The effect of permeability of natural emergent vegetation on floodplain flow, in: Proceedings of the 32nd IAHR World Congress, Venice, Italy, 2007.

[62] H. M. Nepf, E. R. Vivoni, Flow structure in depth-limited, vegetated flow, J. Geophys. Res. 105 (C12) (2000) 28547–28557. doi:10.1029/2000JC900145.

[63] L. E. Frostick, R. E. Thomas, M. F. Johnson, S. P. Rice, S. J. McLelland (Eds.), Users Guide to Ecohydraulic Modelling and Experimentation: Experience of the Ecohydraulic Research Team (PISCES) of the HYDRALAB Network, CRC Press/Balkema, Leiden, The Netherlands, 2014.

[64] M. C. Stone, L. Chen, S. K. McKay, J. Goreham, K. Acharya, C. Fischenich, A. B. Stone, Bending of submerged woody riparian vegetation as a function of hydraulic flow conditions, River Res. Applic. 29 (2) (2013) 195–205. doi:10.1002/rra.1592.

[65] J. Kim, V. Y. Ivanov, N. D. Katopodes, Hydraulic resistance to overland flow on surfaces with partially submerged vegetation, Water Resour. Res. 48 (10) (2012) W10540. doi:10.1029/2012WR012047.

[66] F. Siniscalchi, V. I. Nikora, Flow-plant interactions in open-channel flows: A comparative analysis of five freshwater plant species, Water Resour. Res. 48 (5) (2012) W05503. doi:10.1029/2011WR011557.

[67] A. N. Sukhodolov, T. A. Sukhodolova, Vegetated mixing layer around a finite-size patch of submerged plants: Part 2. Turbulence statistics and structures, Water Resour. Res. 48 (12) (2012) W12506. doi:10.1029/2011WR011805.

[68] I. Nezu, Open-channel flow turbulence and its research prospect in the 21st century, J. Hydraul. Eng. 131 (4) (2005)

229–246. doi:10.1061/(ASCE)0733-9429(2005)131:4(229).

[69] D. G. Goring, V. I. Nikora, Despiking acoustic Doppler velocimeter data, J. Hydraul. Eng. 128 (1) (2002) 117–126. doi:10.1061/(ASCE)0733-9429(2002)128:1(117).

[70] N. Mori, T. Suzuki, S. Kakuno, Noise of acoustic doppler velocimeter data in bubbly flows, J. Eng. Mech. 133 (1) (2007) 122–125. doi:10.1061/(ASCE)0733-9399(2007)133:1(122).

[71] B. M. Sumer, J. Fredsoe, Hydrodynamics around Cylindrical Structures, Vol. 12 of Advanced Series on Ocean Engineering, World Scientific, 1997.

[72] C. Toney, M. C. Reeves, Equations to convert compacted crown ratio to uncompacted crown ratio for trees in the interior west, West. J. Appl. For. 24 (2) (2009) 76–82.

[73] J. V. Ward, K. Tockner, D. B. Arscott, C. Claret, Riverine landscape diversity, Freshwater Biol. 47 (4) (2002) 517–539. doi:10.1046/j.1365-2427.2002.00893.x.

[74] S. Karrenberg, J. Kollmann, P. J. Edwards, A. M. Gurnell, G. E. Petts, Patterns in woody vegetation along the active zone of a near-natural Alpine river, Basic Appl. Ecol. 4 (2) (2003) 157–166. doi:10.1078/1439-1791-00123.

[75] S. J. Vreugdenhil, K. Kramer, T. Pelsma, Effects of flooding duration, -frequency and -depth on the presence of saplings of six woody species in north-west Europe, For. Ecol. Manag. 236 (1) (2006) 47–55. doi:10.1016/j.foreco.2006.08.329.

[76] V. J. Monleon, D. Azuma, D. Gedney, Equations for predicting uncompacted crown ratio based on compacted crown ratio and tree attributes, West. J. Appl. For. 19 (4) (2004) 260–267.

[77] K. C. Randolph, Equations relating compacted and uncompacted live crown ratio for common tree species in the south, South. J. Appl. For. 34 (3) (2010) 118–123.

[78] T. B. Lynch, C. Budhathoki, R. F. Wittwer, Relationships between height, diameter, and crown for eastern cottonwood (populus deltoides) in a Great Plains riparian ecosystem, West. J. Appl. For. 27 (4) (2012) 176–186. doi:10.5849/wjaf.11-030.

[79] C. Hill, M. Musa, L. Chamorro, C. Ellis, M. Guala, Local scour around a model hydrokinetic turbine in an erodible channel, J. Hydraul. Eng. 140 (8) (2014) 04014037. doi:10.1061/(ASCE)HY.1943-7900.0000900.

[80] L. Zong, H. Nepf, Vortex development behind a finite porous obstruction in a channel, J. Fluid Mech. 691 (2012) 368–391. doi:10.1017/jfm.2011.479.

[81] V. Kitsikoudis, O. Yagci, V. S. O. Kirca, D. Kellecioglu, Experimental investigation of channel flow through idealized isolated tree-like vegetation, Environ. Fluid Mech. (Resubmitted after revision).

[82] M. S. Yalin, E. Karahan, Inception of sediment transport, J. Hydraul. Div. 105 (11) (1979) 1433–1443.

[83] Y. Mao, The interaction between a pipeline and an erodible bed, Ph.D. thesis, Denmark Technical University (1986).

[84] B. W. Melville, S. E. Coleman, Bridge Scour, Water Resources Publication, LLC, CO, USA, 2000.

[85] T. Takemura, N. Tanaka, Flow structures and drag characteristics of a colony-type emergent roughness model mounted on a flat plate in uniform flow, Fluid Dyn. Res. 39 (9-10) (2007) 694–710.

doi:10.1016/j.fluiddyn.2007.06.001.

[86] N. Tanaka, J. Yagisawa, Flow structures and sedimentation characteristics around clump-type vegetation, J. Hydro-Environ. Res. 4 (1) (2010) 15–25. doi:10.1016/j.jher.2009.11.002.

[87] V. Kitsikoudis, O. Yagci, V. S. O. Kirca, D. Kellecioglu, Flow field alteration due to permeability and subcanopy flow for emergent vegetation, in: Proc. 26th ISOPE Conference, Rhodes, Greece, 2016.

[88] A. F. Lightbody, H. M. Nepf, Prediction of velocity profiles and longitudinal dispersion in salt marsh vegetation, Limnol. Oceanogr. 51 (1) (2006) 218–228. doi:10.4319/lo.2006.51.1.0218.

[89] J. Jarvela, Flow resistance of flexible and stiff vegetation: a flume study with natural plants, J. Hydrol. 269 (1-2) (2002) 44–54. doi:10.1016/S0022-1694(02)00193-2.

[90] C. A. M. E. Wilson, T. Stoesser, P. D. Bates, A. Batemann Pinzen, Open channel flow through different forms of submerged flexible vegetation, J. Hydraul. Eng. 129 (11) (2003) 847–853. doi:10.1061/(ASCE)0733-9429(2003)129:11(847).

[91] M. Righetti, Flow analysis in a channel with flexible vegetation using double-averaging method, Acta Geophys. 56 (3) (2008) 801–823. doi:10.2478/s11600-008-0032-z.

[92] S. F. Majd, O. Yagci, V. S. O. Kirca, V. Kitsikoudis, E. Lentsiou, Flow and turbulence around an inclined pile, in: 26th ISOPE Conference, Rhodes, Greece, 2016.

[93] M. Fathi-Maghadam, N. Kouwen, Nonrigid, nonsubmerged, vegetative roughness on floodplains, J. Hydraul. Eng. 123 (1) (1997) 51–57. doi:10.1061/(ASCE)0733-9429(1997)123:1(51).